

# Efficient URLLC with a Reconfigurable Intelligent Surface and Imperfect Device Tracking

Fabio Saggese\*, Federico Chiariotti†, Kimmo Kansanen\*‡, and Petar Popovski\*

\*Department of Electronic Systems, Aalborg University, Denmark ({fasa, fchi, kimkan, petarp}@es.aau.dk)

† Department of Information Engineering, University of Padova, Italy

‡Department of Electronic Systems, Norwegian University of Science and Technology

**Abstract**—The use of Reconfigurable Intelligent Surface (RIS) technology to extend coverage and allow for better control of the wireless environment has been proposed in several use cases, including Ultra-Reliable Low-Latency Communications (URLLC) communications. However, the extremely challenging latency constraint makes explicit channel estimation difficult, so positioning information is often used to configure the RIS and illuminate the receiver device. In this work, we analyze the effect of imperfections in the positioning information on the reliability, deriving an upper bound to the outage probability. We then use this bound to perform power control, efficiently finding the minimum power that respects the URLLC constraints under positioning uncertainty. The optimization is conservative, so that all points respect the URLLC constraints, and the bound is relatively tight, with an optimality gap between 1.5 and 4.5 dB.

**Index Terms**—Reconfigurable intelligent surfaces, URLLC, power control, stochastic optimization

## I. INTRODUCTION

A growing body of research has recognized the potential of Reconfigurable Intelligent Surfaces (RISs) to provide improvements in wireless communications by imposing low-power real-time control on the propagated wireless signals [1]. As such, it can result in various performance benefits, such as improved coverage, increased data rate, and mitigation of multi-user interference [1], [2].

Intuitively, a RIS is a good match for Ultra-Reliable Low-Latency Communications (URLLC), since it can act as a full-duplex relay. It can thus support two-way exchanges without incurring additional latency, as there is no need to change the configuration when the communication direction is changed. Nevertheless, the RIS configuration needs to be optimized in order to create a favorable wireless channel between the nodes of interest [2]. The potential of RIS in the context of URLLC has been analyzed in [3], where the authors prove that the reliability of the system is improved by adding an RIS. Other works on the topic focus on the optimization of the system: in [4], the authors design a low-complexity joint beamforming and phase shift optimization algorithm; in [5], the authors propose a grant-free uplink access paradigm based on a mix of resource allocation schemes and receiver design. However,

This work was partly supported by the Villum Investigator grant “WATER” from the Villum Foundation, Denmark, and by the Horizon 2020 “RISE-6G” project, financed by the European Commission under grant no. 101017011.

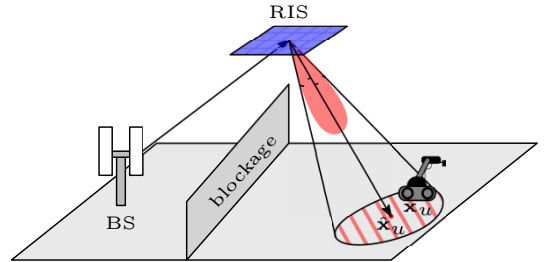


Fig. 1. Scenario of interest.

the above literature is conditioned on the knowledge of the Channel State Information (CSI). In real systems, RIS channel estimation procedures have a complexity proportional to the number of RIS elements [6], [7], and are not practical for URLLC traffic, as the procedure can add a significant delay.

A possible alternative, especially in cases where a strong Line of Sight (LoS) component dominates the propagation, is to use the positioning information of the terminals to configure the RIS beamformer to illuminate the receiver [8]. However, available position information is subject to uncertainty, and, hence, robust optimizations accounting for such error are needed. A formal analysis on the statistical relation between reliability and uncertainty for a generic communication system is carried out in [9]. A design of RIS phase shift optimization taking into account such uncertainty to maximize the average spectral efficiency with no reliability constraint (which makes it unsuitable for URLLC) is presented in [10].

This paper addresses the problem of URLLC communication when the RIS is configured to beam energy towards a User Equipment (UE) based on the tracking of its position at the Base Station (BS). The setup is depicted in Fig. 1, in which the BS transmits in the downlink. For the depicted UE, the dominant portion of the wireless signal arrives through a *controllable* path, which the RIS can affect by changing its configuration. The uncertainty of the UE’s position is due to the noisy tracking process, which is often based on Kalman or particle filters. We propose a method that embeds the position uncertainty into the overall URLLC reliability requirement, determines the RIS configuration and sets the BS transmit power to meet the reliability constraint.<sup>1</sup>

<sup>1</sup>The simulation code for the paper is available at <https://github.com/AAU-CNT/efficient-ris-aided-urllc>

The rest of the paper is divided as follows: first, Sec. II presents the system model. The reliability bound and power optimization are derived in Sec. III, and numerical performance results are described in Sec. IV. Finally, Sec. V concludes the paper and presents some possible avenues of future work.

*Notation:*  $\text{mod}(a, M)$  is the  $a$  modulo  $M$  operation;  $\lfloor a \rfloor$  represent the nearest lower integer of  $a$ . Lower and upper case boldface letters denote vectors  $\mathbf{x}$  and matrices  $\mathbf{X}$ , respectively; the Euclidean norm of  $\mathbf{x}$  is  $\|\mathbf{x}\|$ .  $\mathcal{P}(e)$  is the probability that event  $e$  occurs;  $\mathcal{CN}(\boldsymbol{\mu}, \mathbf{R})$  is the complex Gaussian distribution with mean  $\boldsymbol{\mu}$  and covariance matrix  $\mathbf{R}$ ;  $\mathcal{R}(K, \Omega)$  is the Rice distribution with shape parameter  $K$  and scale parameter  $\Omega$ ;  $\mathbb{E}[\cdot]$  is the expected value operation.

## II. SYSTEM MODEL

We consider an industrial Downlink (DL) URLLC communication scenario in which a single-antenna BS has to communicate to a single-antenna mobile UE. To ensure full coverage, a  $N$ -element RIS is deployed on the ceiling of the factory. We define the three-dimensional coordinate system  $O_1$ , whose origin lies in the center of the RIS  $\mathbf{x}_r = (0, 0, 0)^\top$ . The  $x$  and  $y$  axes are parallel to the horizontal dimensions of the RIS, and the  $z$  axis points towards the floor of the factory. A depiction of coordinate system  $O_1$  is given in Fig. 2.

It is assumed that there is a known one-to-one mapping between the locations of the UE and the RIS configurations. For the propagation scenario in this paper, the mapping is explicitly available as analytical expressions. In the considered industrial scenario with more complicated propagation characteristics, the availability of the mapping implies that a suitable calibration process has taken place, which can map the regions of the floor in which the RIS provides a significant benefit, as the direct path between BS and UE is blocked or weak.

### A. Communication System Model

The available space for the UE is delimited by a square floor of area  $D^2$  m<sup>2</sup> and the ceiling is at a height of  $h$  m. The position of the BS is  $\mathbf{x}_b = (x_b, y_b, z_b)^\top$ , and a LoS path with the RIS exists. The UE moves around the factory floor, so that its coordinates at time  $t$  are  $\mathbf{x}_u(t) = (x_u(t), y_u(t), h)^\top$ . Assuming a square RIS for simplicity of presentation, each element has position on  $O_1$  given by  $\mathbf{r}_n = d(\text{mod}(n-1, \sqrt{N}) - \frac{\sqrt{N}-1}{2}, \lfloor \frac{n-1}{\sqrt{N}} \rfloor - \frac{\sqrt{N}-1}{2}, 0)^\top$  where  $d < \lambda$  is the spacing between the center of neighboring elements and  $\lambda$  is the carrier wavelength. We assume  $h \geq \frac{2}{\lambda}d^2N^2$  in order to assure far-field propagation regardless the position of the UE. Each RIS element influences the incoming signal by inducing a phase shift  $\phi_n$ , and we assume that the attenuation imposed by each element of the RIS is strictly equal to 1. The vector containing the phase shifts of each RIS element is denoted as  $\boldsymbol{\phi} = [e^{j\phi_1}, \dots, e^{j\phi_N}]^\top$ , and it is referred as *phase profile* or *configuration* in the remainder of the paper. The RIS phase profile is controlled by the BS, which receives information about UEs positioning through an out-of-band control channel.

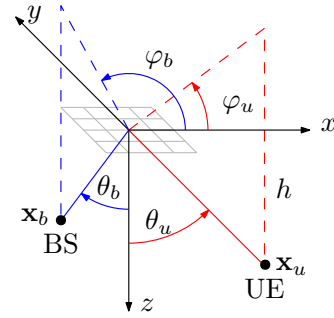


Fig. 2. Coordinate system  $O_1$  of the scenario.

The aim of the BS is then to optimize its own transmitting power and the RIS phase profile to communicate efficiently to the UE while respecting the URLLC constraints.

We assume that the BS tracks the UE's movements through a Kalman-like filter [11], which is a common assumption in indoor and outdoor tracking applications [12], so that the Probability Density Function (PDF) of the estimated position of the UE at time  $t$  is a bivariate Gaussian random variable:

$$p_{\hat{\mathbf{x}}_u(t)}(\mathbf{x}) = \frac{1}{2\pi|\boldsymbol{\Sigma}(t)|} e^{-\frac{1}{2}(\mathbf{x}-\hat{\mathbf{x}}_u(t))^\top \boldsymbol{\Sigma}(t)^{-1}(\mathbf{x}-\hat{\mathbf{x}}_u(t))}, \quad (1)$$

where  $\hat{\mathbf{x}}_u(t)$  is the estimated position at time  $t$  and  $\boldsymbol{\Sigma}(t)$  is the covariance matrix of the Kalman filter.

We can convert the UE's and BS' positions from Cartesian to spherical coordinates  $\mathbf{z}_u(t) = (r_u(t), \theta_u(t), \varphi_u(t))^\top$ , and  $\mathbf{z}_b(t) = (r_b(t), \theta_b(t), \varphi_b(t))^\top$  using the RIS's center as the center of the sphere. The three coordinates represent the radius  $r_i \in [0, \sqrt{D^2/2 + h^2}]$  from the center to the RIS to the user (BS), the elevation angle  $\theta_i \in [-\pi/2, \pi/2]$  computed from the  $z$  axis to the UE's (BS') position, and the azimuth angle  $\varphi_i \in [0, 2\pi]$  identifying the point on the  $x-y$  plane, respectively, with  $i \in \{b, u\}$ . In the following, we omit the time index  $t$  for brevity.

Assuming a transmission bandwidth well below the channel coherence bandwidth, each transmitted symbol will experience a channel which depends on the position of the UE and the BS, the RIS configuration loaded in that moment, and the frequency flat short term fading. Without loss of generality, we assume that the BS transmits a single symbol  $x$  with power  $P$  towards the UE; the received signal can be modeled as

$$y = \sqrt{\beta(\mathbf{x}_u)} P g_b g_u \mathbf{a}_b^\top \text{diag}(\boldsymbol{\phi}) \mathbf{a}_u x + n, \quad (2)$$

where  $|g_b|, |g_u| \sim \mathcal{R}(K, 1)$  are the short term fading realizations for the BS-RIS and RIS-UE paths, and  $n \sim \mathcal{CN}(0, \sigma^2)$  is the receiver noise. The path loss term is given by

$$\beta(\mathbf{x}_u) = \beta_0^2 G_b G_u \left( \frac{d_0^2}{\|\mathbf{x}_u\| \|\mathbf{x}_b\|} \right)^\xi, \quad (3)$$

where  $\beta_0$  is the path loss at a reference distance  $d_0$ ,  $G_b$  and  $G_u$  are the antenna gain of the BS and UE, respectively;  $\xi$  is the path loss exponent. Note that  $\beta_0$  and  $d_0$  are squared due to the double path BS-RIS and RIS-UE. The steering vectors  $\mathbf{a}_b$  and  $\mathbf{a}_u$  represent the angle of arrival from the BS to each

RIS element and the angle of departure from each element to the UE, respectively. The steering vectors are:

$$[\mathbf{a}_i]_n = e^{j\frac{2\pi}{\lambda} \frac{\mathbf{x}_i^T \mathbf{r}_n}{\|\mathbf{x}_i\|}} = e^{j\frac{2\pi}{\lambda} (r_{n,1} \sin \theta_i \cos \varphi_i + r_{n,2} \sin \theta_i \sin \varphi_i)}, \quad (4)$$

with  $i \in \{b, u\}$ . The Signal to Noise Ratio (SNR) is then:

$$\gamma = \frac{P}{\sigma^2} \beta |g_b g_u|^2 N^2 |A(\phi|\hat{\mathbf{x}}_u, \mathbf{x}_u)|^2, \quad (5)$$

where  $A(\phi|\hat{\mathbf{x}}_u, \mathbf{x}_u) = \frac{1}{N} \mathbf{a}_b^T \text{diag}(\phi) \mathbf{a}_u$  denotes the RIS array factor (AF), while  $|A(\phi|\hat{\mathbf{x}}_u, \mathbf{x}_u)|^2$  denotes the AF gain.

### B. Array Factor: Pointing and Beamwidth

We define two indexes spanning through the RIS elements in the horizontal ( $x$ ) and vertical ( $y$ ) dimensions as  $\ell = \text{mod}(n-1, \sqrt{N})$  and  $k = \lfloor \frac{n-1}{\sqrt{N}} \rfloor$ , respectively, and rewrite the AF as

$$A(\phi|\hat{\mathbf{x}}_u, \mathbf{x}_u) = \frac{1}{N} \sum_{\ell=0}^{\sqrt{N}-1} \sum_{k=0}^{\sqrt{N}-1} e^{j\phi_{\ell,k}} \cdot e^{j\frac{2\pi}{\lambda} d \left( \ell - \frac{\sqrt{N}-1}{2} \right) (\sin \theta_u \cos \varphi_u + \sin \theta_b \cos \varphi_b)} \cdot e^{j\frac{2\pi}{\lambda} d \left( k - \frac{\sqrt{N}-1}{2} \right) (\sin \theta_u \sin \varphi_u + \sin \theta_b \sin \varphi_b)}, \quad (6)$$

where  $\phi_{\ell,k} = \phi_n$  using the appropriate index. Without loss of generality, the phase shift impressed by each element can be expressed as  $\phi_{\ell,k} = \ell\phi_x + k\phi_y$ . In this way, we can compensate for the (known) position of the BS, while pointing toward the direction given by  $\hat{\theta}$  and  $\hat{\varphi}$ , by setting

$$\begin{aligned} \phi_x &= -\frac{\pi d}{\lambda} \left( \sin \hat{\theta} \cos \hat{\varphi} + \sin \theta_b \cos \varphi_b \right), \\ \phi_y &= -\frac{\pi d}{\lambda} \left( \sin \hat{\theta} \sin \hat{\varphi} + \sin \theta_b \sin \varphi_b \right). \end{aligned} \quad (7)$$

Inserting (7) into (6), the AF can be rewritten as [13]

$$A(\phi|\hat{\mathbf{x}}_u, \mathbf{x}_u) = \frac{e^{j\frac{\sqrt{N}-1}{2}(\phi_x + \phi_y)}}{N} \frac{\sin(\sqrt{N}f_x)}{\sin(f_x)} \frac{\sin(\sqrt{N}f_y)}{\sin(f_y)}, \quad (8)$$

with  $f_x = \frac{\pi d}{\lambda} (\sin \theta_u \cos \varphi_u - \sin \hat{\theta} \cos \hat{\varphi})$  and  $f_y = \frac{\pi d}{\lambda} (\sin \theta_u \sin \varphi_u - \sin \hat{\theta} \sin \hat{\varphi})$ . If perfect knowledge of the UE's position is available, a trivial solution to maximize the AF is to set  $\hat{\theta} = \theta_u$ ,  $\hat{\varphi} = \varphi_u$ ; however, a positioning error is always present. Therefore, we resort to evaluate the illuminated region (on the floor)  $\mathcal{G}(A_0)$  in which the AF gain is at least equal to  $A_0$  after setting  $\hat{\theta} = \hat{\theta}_u$ ,  $\hat{\varphi} = \hat{\varphi}_u$ .

The AF of a square Uniform Planar Array (UPA) when pointing toward the direction given by  $\hat{\theta}$  and  $\hat{\varphi}$ , i.e.,  $\hat{\mathbf{w}} = (\sin \hat{\theta} \cos \hat{\varphi}, \sin \hat{\theta} \sin \hat{\varphi}, \cos \hat{\theta})^T$  is given by (8). The 3D beamwidth generating an AF gain of  $A_0 \in (0, 1]$  can then be approximated by the angles [13, Section 6.10]

$$\Delta\theta(A_0) = \frac{\Delta\Theta(A_0)}{\cos \hat{\theta}}, \quad \Delta\varphi(A_0) = \Delta\Theta(A_0). \quad (9)$$

Thus, the points in the 3D space with an AF gain of  $A_0$  lie on the surface of an elliptic cone whose vertical axis is the pointing direction  $\hat{\mathbf{w}}$ , the major diameter ( $2a$ ) is generated

by the angle  $\Delta\theta(A_0)$  in the elevation plane is defined by  $\varphi = \hat{\varphi}$ , and the minor diameter ( $2b$ ) is generated by the angle  $\Delta\theta(A_0)$  on the plane perpendicular to the elevation one (see [13, Fig. 6.38]). In (9),  $\Delta\Theta(A_0)$  is the beamwidth of the Uniform Linear Array (ULA) spanning through the  $x$  (or  $y$ ) dimension providing an AF gain of  $A_0$ , whose approximation is given in the following proposition.

**Proposition 1.** *The beamwidth of a ULA given an AF target gain  $A_0$  can be approximated as*

$$\Delta\Theta(A_0) \approx \arcsin \left( 2 \frac{\lambda x(A_0)}{\pi d \sqrt{N}} \right), \quad (10)$$

where  $x(A_0) = \{x \mid \text{sinc}(x) = A_0\}$ .

*Proof.* In the main lobe, the ULA AF is  $\approx \text{sinc}(\sqrt{N}f_x)$  [13], where  $\varphi = \hat{\varphi} = 0$  because the elements span the  $x$  axis. Neglecting the pointing effect, i.e.,  $\hat{\theta} = \pi/2$ , and solving  $\sqrt{N}f_x = x(A_0)$  with respect to  $\theta$  completes the proof.  $\square$

The arguments  $x(A_0)$  can be easily obtained by numerical simulations for the desired values of  $A_0$ .

### III. POWER CONTROL FOR URLLC

While most URLLC packets are short, the finite blocklength effects disappear when only statistical knowledge of the CSI is available, as proven in [14]. Hence, we can use Shannon's capacity formula to derive the minimum required SNR to reliably deliver the data, and perform power control for the URLLC transmission. If we consider a packet of length  $L$  bits, which has to be transmitted with a maximum latency  $T$  over bandwidth  $B$ , the minimum required SNR  $\gamma_0$  is

$$\gamma_0 = 2^{\frac{L}{BT}} - 1. \quad (11)$$

The actual SNR in (5) includes two independent random components: the first is the fading, which is given by the product of the fading on the BS-RIS and RIS-UE channels, while the second depends on the actual position of the UE. If the UE's coordinates are given by  $\mathbf{x}_u$ , the average SNR  $\hat{\gamma}(\hat{\mathbf{x}}_u, \mathbf{x}_u)$  is given by:

$$\hat{\gamma}(\hat{\mathbf{x}}_u, \mathbf{x}_u) = \frac{P}{\sigma^2} \beta(\mathbf{x}_u) \mathbb{E}[|g_m g_b|^2] N^2 |A(\phi|\hat{\mathbf{x}}_u, \mathbf{x}_u)|^2, \quad (12)$$

and we know that  $\mathbb{E}[|g_m g_b|^2] = 1$ . The two random terms (the fading and the UE's position) can be considered as independent. The BS can then optimize the transmission power  $P$  to minimize energy consumption while meeting the URLLC requirements.

The intuition for our procedure is the following: first, we find an upper bound to the outage probability by considering either a deep fading event or a large positioning error as a failure (without computing the intersection, or the possibility that a lucky fading gain might compensate for a larger positioning error). We then try to find the minimum gain that allows the resulting beam to illuminate the region in which the UE might be, and invert the resulting values to find a transmission power that ensures URLLC constraints are met.

### A. Reliability Bound

The overall problem is complex, as the distribution of the instantaneous SNR is extremely difficult and must be obtained numerically, making the computation difficult: as URLLC requirements limit the computational effort that can be spent in optimizing the system before transmission, this makes a direct calculation infeasible. However, we can compute a lower bound to reliability by separating the two components:

**Theorem 1.** Let  $G_0 > 0$  be a positive value. If  $\mathcal{P}(|g_u g_b|^2 \leq G_0) = \delta$ , we have:

$$\mathcal{P}(\gamma < \gamma_0) \leq \delta + \mathcal{P}\left(\hat{\gamma} \leq \frac{\gamma_0}{G_0}\right). \quad (13)$$

*Proof.* We can consider two cases:

- 1) In the first case,  $|g_u g_b|^2 > G_0$ . We can then express the following bound:

$$\gamma = \hat{\gamma} |g_u g_b|^2 > \hat{\gamma} G_0. \quad (14)$$

If  $\hat{\gamma} G_0 \geq \gamma_0$ , we then always have  $\gamma \geq \gamma_0$ , and in this case we have:

$$\mathcal{P}(\gamma < \gamma_0 | G_0 < |g_u g_b|^2) \leq \mathcal{P}(\hat{\gamma} G_0 < \gamma_0). \quad (15)$$

- 2) In the second case,  $|g_u g_b|^2 \leq G_0$ , and  $\mathcal{P}(\gamma < \gamma_0 | G_0 \leq |g_u g_b|^2) \leq 1$  (which is trivially true).

By definition, the first and second case are mutually exclusive, and occur with probability  $1 - \delta$  and  $\delta$ , respectively. By applying the law of total probability, the overall probability  $\mathcal{P}(\gamma < \gamma_0)$  is upper bounded by  $\delta + (1 - \delta)\mathcal{P}(G_0 \hat{\gamma} < \gamma_0)$ . As  $\delta \leq 1$ , the theorem is proven.  $\square$

We can then consider power control, applying the bound in the first theorem to find the power requirement.

**Theorem 2.** Let  $\mathcal{G}(A_0) : \{\mathbf{x} \in \mathbb{R}^2 : |A(\phi|\hat{\mathbf{x}}_u, \mathbf{x})|^2 \geq A_0\}$  be the set of points for which the AF gain is larger than  $A_0$ , and let  $\varepsilon = \mathcal{P}(\mathbf{x}_u \in \mathcal{G}(A_0) | \hat{\mathbf{x}}_u, \Sigma_u)$  be the probability that the UE is inside the set. As above, let  $G_0 > 0$  be a positive value so that  $\mathcal{P}(|g_u g_b|^2 \leq G_0) = \delta$ . We then have:

$$\mathcal{P}(\gamma < \gamma_0) \leq \delta + \varepsilon, \quad \forall P \geq \frac{\sigma^2 \gamma_0}{N^2 G_0 A_0 \min_{\mathbf{x} \in \mathcal{G}(A_0)} \beta(\mathbf{x})}. \quad (16)$$

*Proof.* We know that the average SNR in a certain position is given by (12). If we consider a point in  $\mathcal{G}(A_0)$ , the average SNR is lower bounded by:

$$\hat{\gamma}(\hat{\mathbf{x}}_u, \mathbf{x}_u) \geq \frac{P}{\sigma^2} N^2 A_0 \min_{\mathbf{x} \in \mathcal{G}(A_0)} \beta(\mathbf{x}), \quad \forall \mathbf{x}_u \in \mathcal{G}(A_0). \quad (17)$$

Since the result above is a lower bound, we can divide the two cases:

- 1) If  $\mathbf{x}_u \in \mathcal{G}(A_0)$ , we can set a value  $P$  that ensures  $G_0 \hat{\gamma} > \gamma_0$  by applying the lower bound:

$$P \geq \frac{\sigma^2 \gamma_0}{N^2 G_0 A_0 \min_{\mathbf{x} \in \mathcal{G}(A_0)} \beta(\mathbf{x})}. \quad (18)$$

We then have  $\mathcal{P}(G_0 \hat{\gamma} < \gamma_0 | \mathbf{x}_u \in \mathcal{G}(A_0)) = 0$  for all power levels that satisfy the condition.

- 2) If  $\mathbf{x}_u \notin \mathcal{G}(A_0)$ , we consider the packet as lost, i.e., we use the trivial bound  $\mathcal{P}(G_0 \hat{\gamma} < \gamma_0 | \mathbf{x}_u \notin \mathcal{G}(A_0)) \leq 1$ . By definition, this case occurs with probability  $\varepsilon$ .

We then apply Theorem 1 and the law of total probability:

$$\begin{aligned} \mathcal{P}(\gamma < \gamma_0) &\leq \delta + \mathcal{P}\left(\hat{\gamma} \leq \frac{\gamma_0}{G_0}\right) \\ &= \delta + \varepsilon \mathcal{P}\left(\hat{\gamma} \leq \frac{\gamma_0}{G_0} \mid \mathbf{x}_u \notin \mathcal{G}(A_0)\right) \\ &\quad + (1 - \varepsilon) \mathcal{P}\left(\hat{\gamma} \leq \frac{\gamma_0}{G_0} \mid \mathbf{x}_u \in \mathcal{G}(A_0)\right) \leq \delta + \varepsilon, \end{aligned} \quad (19)$$

completing the proof.  $\square$

### B. Beam Projection

We now find a closed-form expression for region  $\mathcal{G}(A_0)$ . The region in 3D space that has an AF gain larger than  $A_0$  is an elliptic cone, whose axis is the line between the RIS and  $\hat{\mathbf{x}}_u$  and whose base is an ellipse whose axes are defined by the two beamwidth parameters from (9). The projection of this elliptic cone on the plane defined by the floor defines  $\mathcal{G}(A_0)$ .

We can write the equation of the cone in a standard form employing a new coordinate system  $O_2$ .  $O_2$  is such that the  $w$  axis is the cone's vertical axis, and  $u$  and  $v$  axes are parallel to the major and minor axis of the ellipse, respectively. The rotation matrix of the transformation from  $O_1$  to  $O_2$  is

$$\mathbf{R} = \begin{pmatrix} -\cos \hat{\theta} \cos \hat{\varphi} & -\cos \hat{\theta} \sin \hat{\varphi} & \sin \hat{\theta} \cos \hat{\varphi} \\ \sin \hat{\varphi} & -\cos \hat{\varphi} & 0 \\ \sin \hat{\theta} \cos \hat{\varphi} & \sin \hat{\theta} \sin \hat{\varphi} & \cos \hat{\theta} \end{pmatrix}. \quad (20)$$

Hence, the point on the floor (i.e.,  $z = h$ ) in  $O_1$  can be represented in  $O_2$  following the relation

$$\begin{pmatrix} u & v & w \end{pmatrix}^T = \mathbf{R} \begin{pmatrix} x & y & z \end{pmatrix}^T. \quad (21)$$

Using coordinate system  $O_2$ , the equation for the cone is

$$\frac{u^2}{a^2} + \frac{v^2}{b^2} = w^2, \quad (22)$$

where  $a$  and  $b$  can be computed from the definition of the 3D beamwidth angles given in (9) at reference distance  $w = 1$ :

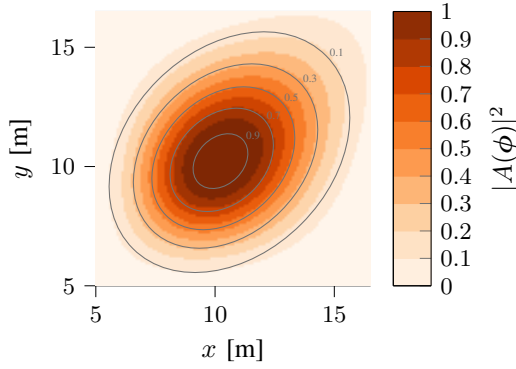
$$a = \tan(\Delta\theta(A_0)/2), \quad b = \tan(\Delta\varphi(A_0)/2). \quad (23)$$

Therefore, we can substitute (21) into (22) and compute the equation of the intersection of the cone with the floor, i.e.,

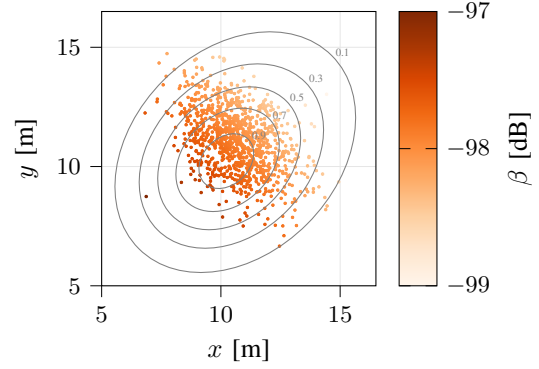
$$\begin{cases} Ax^2 + Bxy + Cy^2 + Dx + Ey + F = 0; \\ z = h. \end{cases} \quad (24)$$

where the parameters indicated by capital letters are given by:

$$\begin{cases} A = \cos^2 \hat{\varphi} (a^{-2} \cos^2 \hat{\theta} - \sin^2 \hat{\theta}) + b^{-2} \sin^2 \hat{\varphi} \\ B = 2 \cos \hat{\varphi} \sin \hat{\varphi} (a^{-2} \cos^2 \hat{\theta} - b^{-2} - \sin^2 \hat{\theta}) \\ C = \sin^2 \hat{\varphi} (a^{-2} \cos^2 \hat{\theta} - \sin^2 \hat{\theta}) + b^{-2} \cos^2 \hat{\varphi} \\ D = -2h \cos \hat{\theta} \sin \hat{\theta} \cos \hat{\varphi} (a^{-2} \cos \hat{\varphi} + 1) \\ E = -2h \cos \hat{\theta} \sin \hat{\theta} \sin \hat{\varphi} (a^{-2} \cos \hat{\varphi} + 1) \\ F = h^2 (a^{-2} \sin^2 \hat{\varphi} \cos^2 \hat{\varphi} + \cos^2 \hat{\theta}). \end{cases} \quad (25)$$



(a) Heatmap of the AF gain.



(b) Scatter plot of UE positions  $\mathbf{x}_u$ .

Fig. 3.  $\mathcal{G}(A_0)$  for different  $A_0$  using the ellipse approximation with  $h = 25$  m,  $\hat{\varphi} = \pi/4$ ,  $\hat{\theta} = \pi/6$ .

---

### Algorithm 1: Power control optimization.

---

```

1 PowerControl( $B, L, T, N, \sigma, \hat{\mathbf{x}}_u, \Sigma_u, A_{\min}, \delta, \varepsilon, \nu$ )
2  $\gamma_0 \leftarrow 2^{\frac{L}{BT}} - 1$ ;
3  $G_0 \leftarrow \text{FADINGICDF}(\delta)$ ;
4  $A_0 \leftarrow \text{ARRAYFACTOR}(\hat{\mathbf{x}}_u, \Sigma_u, A_{\min}, \varepsilon, \nu)$ ;
5 if  $A_0 > 0$  then
6    $\mathbf{x}_c, a', b' \leftarrow \text{ELLIPSEPARAMETERS}(\hat{\mathbf{x}}_u, A_0)$ ;
7    $\hat{\beta} \leftarrow \text{PATHLOSS}(\mathbf{x}_c + a'(\cos \hat{\varphi}, \sin \hat{\varphi}, 0)^T)$ ;
8    $P \leftarrow \frac{\sigma^2 \gamma_0}{N^2 G_0 A_0 \hat{\beta}}$ ;
9   return  $A_\ell$ ;
10 else
11   return  $-1$ ;

```

---

The center and semi-axes of the projected ellipse are denoted as  $\mathbf{x}_c$ ,  $a'$  and  $b'$ , respectively, and can be easily derived from (24). The ellipse's major semi-axis  $a'$  is rotated by an angle  $\hat{\varphi}$  from the  $x$  axis. Fig. 3a shows the heatmap of the AF gain and the projected ellipses obtained with different values of  $A_0$ : the heatmap shows the real AF gain, while the ellipses drawn on it represent the approximation given above. The approximation is generally good, if slightly pessimistic, guaranteeing that points inside the ellipse will respect the condition on the AF gain.

### C. Iterative Optimization

By using beam projection, we can then compute the region  $\mathcal{G}(A_0)$ , which corresponds to an ellipse, and find the minimum power required in that region. If our goal is to find the minimum power  $P$  that ensures a reliability level  $p_s$ , we can set  $\delta$  and  $\varepsilon$  such that  $\delta + \varepsilon = 1 - p_s$  and run Algorithm 1.

First, the value of  $\gamma_0$  is computed by applying (11), while  $G_0$  is computed in line 3: as the overall fading distribution is determined by the product of two independent Rice fading gains,  $|g_u g_b|^2$ , the inverse Cumulative Density Function (CDF) cannot be computed analytically. However, fading parameters are relatively stable, and can be computed in advance by numerical methods and tabulated, so that the calculation just requires the retrieval of the correct value from a table. Finding the value of  $A_0$  that ensures that  $\mathcal{P}(\mathbf{x}_u \notin \mathcal{G}(A_0)) < \varepsilon$  requires an iterative optimization, which can be performed by binary search. The precision parameter  $\nu$  determines the number of iterations that the search will use, but since  $A_0$  is

---

### Algorithm 2: Reliable AF gain binary search.

---

```

1 ArrayFactor( $\hat{\mathbf{x}}_u, \Sigma_u, A_{\min}, N, \varepsilon, \nu$ )
2  $A_h \leftarrow 1 - \nu$ ;
3  $A_\ell \leftarrow A_{\min}$ ;
4 if  $\text{ELLIPSEPROBABILITY}(\hat{\mathbf{x}}_u, \Sigma_u, A_\ell, N) < 1 - \varepsilon$  then
5   return  $-1$ ;
6 if  $\text{ELLIPSEPROBABILITY}(\hat{\mathbf{x}}_u, \Sigma_u, A_h, N) \geq 1 - \varepsilon$  then
7   return  $1 - \nu$ ;
8 /* Binary search */
9 while  $A_h - A_\ell > \nu$  do
10    $A_0 \leftarrow (A_h + A_\ell)/2$ ;
11    $e \leftarrow \text{ELLIPSEPROBABILITY}(\hat{\mathbf{x}}_u, \Sigma_u, A_0, N)$ ;
12   if  $e < 1 - \varepsilon$  then
13      $A_h \leftarrow A_0$ ;
14   else
15      $A_\ell \leftarrow A_0$ ;
16 return  $A_\ell$ ;

```

---

directly proportional to the required power, we do not need a large number of iterations. Considering a minimum AF gain  $A_{\min} = 0.1$ , which ensures that the illuminated points are still within the main lobe, just 5 iterations allow us to reach a maximum error of 2% on the value of the array factor. If the positioning uncertainty is too large, and even  $\mathcal{G}(A_{\min})$  is too small for  $\varepsilon$ , the URLLC transmission is impossible, and the BS reports this to the application. Taking a pessimistic approach, we consider the minimum viable array factor within this precision, giving us a worst case increase of transmit power of 2%. The full binary search procedure is reported in Algorithm 2: the  $\text{ELLIPSEPROBABILITY}$  function, first used in line 4 of the algorithm, simply computes the probability that the UE will be inside the ellipse by computing the CDF of the position distribution (see Fig. 3b for a visualization of the position realizations and  $\mathcal{G}(A_0)$ ). While the integral of a bivariate Gaussian random variable over an arbitrary ellipse—which is required to get  $\mathcal{P}(\mathbf{x}_u \in \mathcal{G}(A_0))$ —does not have a closed-form solution, it is a well-known numerical problems with several efficient and tabulated solutions [15], [16].

Finally, since  $\mathcal{G}(A_0)$  is approximated by the ellipse computed in the previous section, the maximum attenuation given by the path loss in the region is

$$\min_{\mathbf{x} \in \mathcal{G}(A_0)} \beta(\mathbf{x}) = \beta(\mathbf{x}_c + a'(\cos \hat{\varphi}, \sin \hat{\varphi}, 0)^T). \quad (26)$$



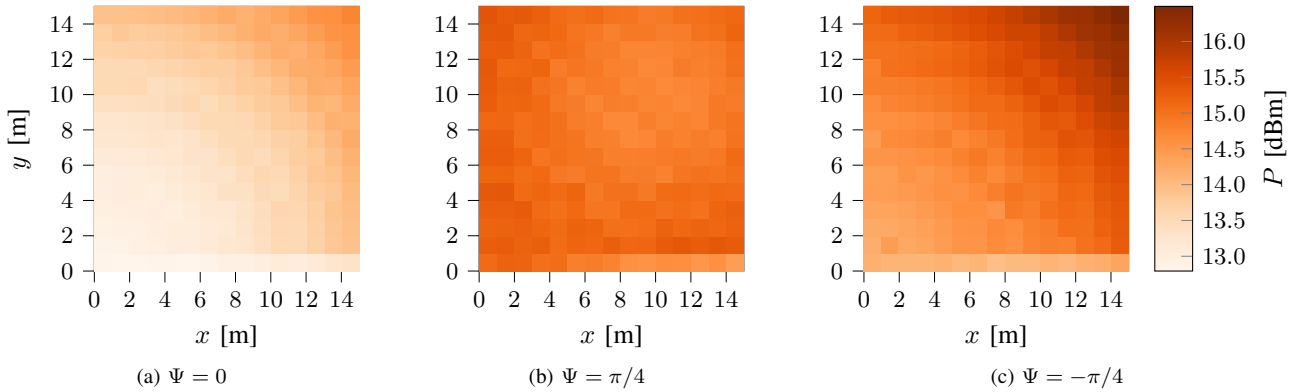


Fig. 4. Power consumption in the first quadrant of the area.

As all numerical steps in the optimization can be tabulated and computed efficiently, and the number of iterations of the binary search is extremely limited; the procedure for power control based on the upper bound can be computed within the URLLC time constraints, even considering the limits of embedded processors installed in BSs.

#### IV. NUMERICAL RESULTS

In this section, we present our numerical results. The parameters we used are listed in Table I, and may refer to a typical URLLC scenario [3], [14]. The values of  $\delta$  and  $\varepsilon$  have been found empirically. We highlight that the deadline to transmit the packet is 0.5 ms, which is stricter than the typical URLLC deadline to allow some time for RIS configuration and power optimization: however, this is still not enough to perform the extensive Monte Carlo simulations that would be required to compute the optimal power. The covariance matrix of the UE's position uncertainty is

$$\Sigma = \sigma_u^2 \begin{bmatrix} \frac{1}{\cos^2 \Psi} & \frac{\sin \Psi}{\sin \Psi} \\ \frac{\sin \Psi}{\sin \Psi} & \frac{1}{\cos^2 \Psi} \end{bmatrix} \quad (27)$$

where  $\sigma_u = 0.3$  m and  $\Psi \in \{0, \pi/4, -\pi/4\}$ . Eq. (27) is used to capture three different user behaviors: when  $\Psi = 0$ , the uncertainty is a circularly symmetric Gaussian representing the error when the user is static; when  $\Psi = \pi/4$  or  $-\pi/4$ , the major axis of the equi-probability ellipse is oriented toward  $\Psi$ , emulating the output error of common tracking filters when the UE is moving in direction  $\Psi$  [17]. The worst-case scenario is when  $\Psi = \pi/2 - \hat{\varphi}$ , as the highest positioning error is aligned with the minor axis of the projected beam ellipse.

Fig. 4 shows a heatmap of power consumption for the three values of  $\Psi$ : we can easily notice that power consumption is generally lower for  $\Psi = 0$ , and that the path loss is still the most important component: points farther away from the origin generally require a higher power. However, the increase is slower than the path loss, as the effect of the positioning error decreases: as  $\hat{\theta}$  increases, the projection of the beam on the floor becomes larger, so the same positioning error distribution is covered by an ellipse associated to a higher AF gain. In the asymmetric error cases, shown in Fig. 4b-c, the effect of  $\hat{\varphi}$  is significant: if  $\Psi = \pi/4$ , the required power is minimal when  $\hat{\varphi} = \Psi$ , i.e., when the projected beam and the

TABLE I  
SIMULATION PARAMETERS.

Parameter	Symbol	Value
<b>Scenario</b>		
Room side	$D$	15 m
Ceiling height	$h$	25 m
BS position	$\mathbf{x}_b$	$(-5, -5, 5)^\top$ m
RIS element spacing	$d$	$\lambda/2$
Number of RIS elements	$N$	100
Positioning error deviation	$\sigma_u$	0.3 m
<b>Communication system</b>		
Packet length	$L$	32 bytes
Wavelength	$\lambda$	0.333 m
Bandwidth	$B$	360 kHz
Latency constraint	$T$	0.5 ms
Reliability	$p_s$	99.999%
Fading shape parameter	$K$	6 dB
UE and BS antenna gains	$G_b \cdot G_u$	12.85 dB
Reference distance	$d_0$	1 m
Path loss exponent	$\xi$	2
Reference path gain	$\beta_0$	-31.53 dB
UE noise power	$\sigma^2$	-94 dBm
Algorithm parameters	$[\delta, \varepsilon]$	$[0.9, 0.1] \cdot (1 - p_s)$

positioning error are aligned, and increases as the two ellipses rotate relative to each other. The opposite happens if  $\Psi = -\pi/4$ , as required power is maximal when the highest position error is orthogonal to the projected beam. Interestingly, the case with  $\Psi = \pi/4$  also requires less power when the UE is farther away: if  $\varphi$  is close to  $\Psi$ , the increased eccentricity of the projection beam better matches the shape of the position distribution, improving the reliable AF gain  $A_0$  enough to offset the increased path loss. Naturally, the opposite happens if  $\Psi = -\pi/4$ .

In order to provide a meaningful comparison, we consider a fixed azimuth angle  $\hat{\varphi} = \pi/4$  and consider performance as a function of  $\hat{\theta} \in [0, 40^\circ]$ , evaluating both the outage probability and power consumption. As a term of comparison, we show the results of an ideal oracle approach obtained by Monte Carlo simulations, referred as OPT in the following. For this solution, the empirical CDF of  $\gamma/P$  is estimated over  $10^7$  realizations of the UE's position and fading, and inverted to find the power that gives exactly  $\mathcal{P}(\gamma \leq \gamma_0) = 1 - p_s$ . Fig. 5 shows the comparison, where the proposed practical power control solution is denoted as PC.

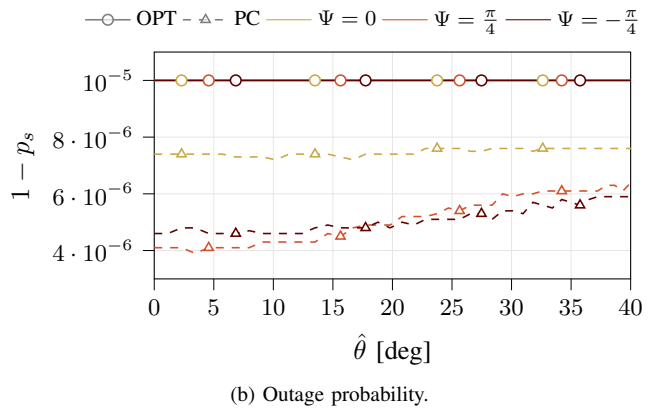
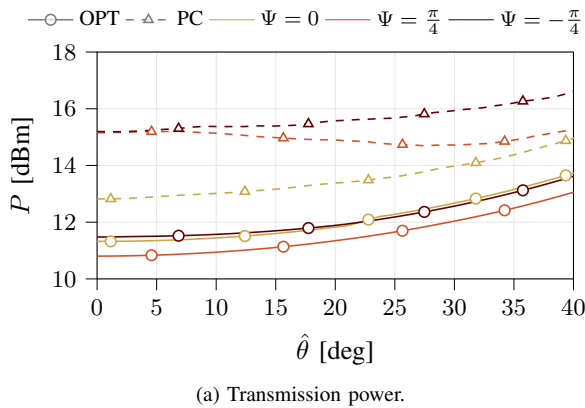


Fig. 5. Performance as a function of  $\hat{\theta}$  with  $\hat{\varphi} = \pi/4$ .

Fig. 5a shows that the proposed solution slightly overestimates the required power, particularly in the cases with  $\Psi = \pm\pi/4$ : the optimality gap is between 1.5 and 4.5 dB, as the upper bound to the outage probability is relatively tight, but still leaves some slack. Fig. 5b confirms the conservative nature of the proposed solution: the outage probability, which should be close to  $10^{-5}$ , is between 25 and 60% lower. It is worth noting that OPT always has an outage probability exactly equal to  $10^{-5}$ , as it obtained by the straightforward inversion of the empirical CDF of  $\gamma/P$ , while, as we remarked above, PC provides the closest performance when the UE is static, ( $\Psi = 0$ ), and the worst performance when the direction of movement is perpendicular to  $\hat{\varphi}$  ( $\Psi = -\pi/4$ ). As we noted above, the increased eccentricity of  $\mathcal{G}(A_0)$  as the elevation angle grows has a positive effect if  $\Psi = \hat{\varphi}$ , and a negative effect in the other two cases. When  $\hat{\theta} \simeq 0$ ,  $\mathcal{G}(A_0)$  is almost circular: asymmetric uncertainty distributions are likelier to generate positions outside the illuminated area. When pointing toward the sides,  $\mathcal{G}(A_0)$  is eccentric in the  $\hat{\varphi}$  direction, and an asymmetric positioning error in the same direction is beneficial (see also Fig. 3b for the  $\Psi = -\pi/4$  case).

## V. CONCLUSION AND DISCUSSION

In this work, we present a method for computationally efficient power control in RIS-assisted URLLC, based on an upper bound to the outage probability which includes position uncertainty. The results show that the optimality gap is relatively small, as the method always meets URLLC requirements with a slightly higher power than the optimum.

Future work can focus on further refining the bounds, as well as considering different localization methods, which may even rely on the RIS itself. Furthermore, an analysis of the calibration process, which the BS uses to learn the locations in which the controllable path is dominating the uncontrollable paths, could be another extension of the paper. The optimization of the sweeping process that gauges the impact of the controllable path in each position in a dynamic environment is an interesting development.

## REFERENCES

- [1] Q. Wu, S. Zhang *et al.*, "Intelligent reflecting surface-aided wireless communications: A tutorial," *IEEE Trans. on Communications*, vol. 69, no. 5, pp. 3313–3351, 2021.
- [2] E. Björnson, H. Wymeersch *et al.*, "Reconfigurable intelligent surfaces: A signal processing perspective with wireless applications," *IEEE Signal Processing Mag.*, vol. 39, no. 2, pp. 135–158, 2022.
- [3] R. Hashemi, S. Ali *et al.*, "Average rate and error probability analysis in short packet communications over RIS-aided URLLC systems," *IEEE Trans. on Vehicular Technology*, vol. 70, no. 10, pp. 10 320–10 334, 2021.
- [4] W. R. Ghanem, V. Jamali *et al.*, "Joint beamforming and phase shift optimization for multicell IRS-aided OFDMA-URLLC systems," in *Wireless Communications and Networking Conf. (WCNC)*. IEEE, 2021.
- [5] D. C. Melgarejo, C. Kalalas *et al.*, "Reconfigurable intelligent surface-aided grant free access for uplink URLLC," in *2nd 6G Wireless Summit*, 2020, pp. 1–5.
- [6] L. Wei, C. Huang *et al.*, "Channel estimation for RIS-empowered multi-user MISO wireless communications," *IEEE Trans. on Communications*, vol. 69, no. 6, pp. 4144–4157, 2021.
- [7] M. Jian, G. C. Alexandropoulos *et al.*, "Reconfigurable intelligent surfaces for wireless communications: Overview of hardware designs, channel models, and estimation techniques," *Intelligent and Converged Networks*, vol. 3, no. 1, pp. 1–32, 2022.
- [8] V. Jamali, G. C. Alexandropoulos *et al.*, "Low-to-zero-overhead IRS reconfiguration: Decoupling illumination and channel estimation," *IEEE Communications Lett.*, vol. 26, no. 4, pp. 932–936, 2022.
- [9] T. Kallehauge, P. Ramirez-Espinosa *et al.*, "A primer on the statistical relation between wireless ultra-reliability and location estimation," *IEEE Wireless Communications Lett.*, vol. 11, no. 8, pp. 1600–1604, 2022.
- [10] A. Abrardo, D. Dardari *et al.*, "Intelligent reflecting surfaces: Sum-rate optimization based on statistical position information," *IEEE Trans. on Communications*, vol. 69, no. 10, pp. 7121–7136, 2021.
- [11] R. Kalman, "A new approach to linear filtering and prediction problems," *Journal of Basic Engineering*, vol. 82, no. 1, pp. 35–45, 1960.
- [12] Z. Vatansever and M. Brandt-Pearce, "Visible light positioning with diffusing lamps using an extended Kalman filter," in *Wireless Communications and Networking Conf. (WCNC)*. IEEE, 2017.
- [13] C. A. Balanis, *Antenna Theory: Analysis and Design*. John Wiley & Sons, 2015.
- [14] G. Durisi, T. Koch *et al.*, "Toward massive, ultra reliable, and low-latency wireless communication with short packets," *Proceedings of the IEEE*, vol. 104, no. 9, pp. 1711–1726, 2016.
- [15] A. Di Donato and M. Jarnagin, "Integration of the general bivariate gaussian distribution over an offset circle," *Mathematics of Computation*, vol. 15, no. 76, pp. 375–382, 1961.
- [16] C. Groenewoud and J. Vitalis, *Bivariate Normal Offset Circle, Probability Tables with Offset Ellipse Transformations*. Cornell Aeronautical Laboratory of Cornell University, 1967.
- [17] H. Li, H. Lu *et al.*, "Toward translating raw indoor positioning data into mobility semantics," *ACM Trans. on Data Science*, vol. 1, no. 4, pp. 1–37, 2020.